ISSN 1063-7842, Technical Physics, 2021, Vol. 66, No. 12, pp. 1341–1347. © Pleiades Publishing, Ltd., 2021.

Mitigation of Thermal Effects in End Pumping of Nd:YAG and Composite YAG/Nd:YAG Laser Crystals, Modelling and Experiments

N. M. Al-Hosiny[a,*], A. A. El-Maaref[b,c], and R. M. El-Agmy[d,]**

[a] *Department of Physics, College of Science, Taif University, P.O. Box 1109, Taif, 21944 Saudi Arabia*
[b] *Department of Physics, Collage of Science, Jouf University, P.O. Box 2014, Skaka, Saudi Arabia*
[c] *Physics Department, Faculty of Science, Al-Azhar University, Assiut, 71524 Egypt*
[d] *Department of Physics, Faculty of Science, Helwan University, Helwan, Cairo, 11792 Egypt*
**e-mail: najm@tu.edu.sa*
***e-mail: Redaagmy@science.helwan.edu.eg*

Received February 16, 2021; revised March 28, 2021; accepted April 4, 2021

Abstract—In this work, we have presented a finite element (FE) numerical modelling simulations to study and analyze the thermal effects in Nd:YAG and composite YAG/Nd:YAG laser rods. We have calculated the temperature distributions, stress intensity and thermal focal lengths at different pump powers for both rods. The FE simulations showed that using composite laser rod of undoped cap reduces the maximum value of stress intensity and thermal focal length by ~35 and ~50%, respectively. We have verified the FE calculations experimentally by direct measurement of focal length of thermally induced lens by using Hartmann–Shack wavefront sensor. Good agreement was obtained between FE calculations and experimental measurements.

DOI: 10.1134/S1063784221080028

1. INTRODUCTION

Diode-pumped Nd:YAG laser has been used as a laser source in many different fields including industrial, medical and scientific research either in a continuous or a pulsed mode [1–4]. Developing Nd:YAG lasers in a sense of low threshold and high beam quality can be accomplished in end pumping configuration [5, 6]. However, in end pumped mode, the pump beam is localized over a small area. Resulting in nonuniform temperature distribution over the cross section of the laser crystal [7].

Accordingly, a nonuniform refractive index is produced as a parabolic-logarithmic function (thermal dispersion dn/dT) [8, 9], bugling of pumped end (end effect) and stress induced birefringence. Thermal dispersion, end effect and stress induced birefringence are responsible for the formation of thermally induced lens and the associated unfavorite effects leading to limitation of pump power, degradation of beam quality and unstable laser resonator, in addition to fracture of laser rod [10–13].

To understand and mitigate all these unfavorite effects, each effect has to be analyzed and mitigated separately since several physical effects contribute at once.

Various attempts have been reported in literature for the compensation of thermally induced lens or stress induced birefringence in diode pumped solid state lasers [14–17]. However, complete compensation of thermally induced lens has not been realized yet in addition to power scaling that imposed but could cause rod fracture.

In this work, we focus on mitigation of heat load and the associated drawbacks for the sake of improving laser performance via composite Nd:YAG laser rod and compared with other Nd:YAG laser rod. We have introduced numerical modelling that makes it possible to investigate complex pumping geometry, cooling techniques and different geometries. The finite element (FE) modelling simulation results, which performed with LASCAD program [18], showed that using composite laser rod of undoped section with neodymium (Nd) is capable for mitigating the focal length of thermally induced lens and stress intensity by 1/3 and 1/2, respectively. We have also performed laser experiment and direct measurement of thermal focal length for both rods using Hartmann–Shack sensor. The comparison between FE calculation and measurements were coincides.

2. PROCESSING OF FE-CODE INFORMATION

In a solid-state laser, at least the energy difference between pump and laser photons is converted to heat.

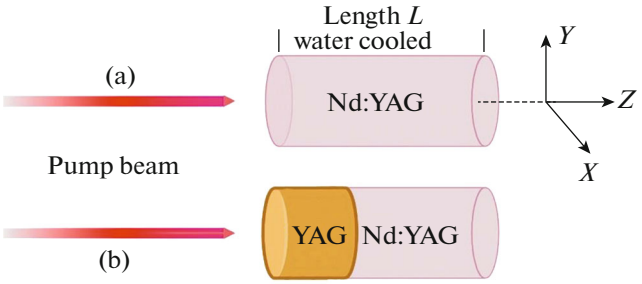

Fig. 1. Sketch of end pumped laser rods (a) Nd:YAG and (b) composite YAG/Nd:YAG.

For continuous-wave (CW) pumping, the 3D temperature profile $T(x, y, z)$ can be found by solving the steady state differential heat equation [19, 20]:

$$\nabla^2 T(x,y,z) + \frac{q(x,y,z)}{k} = 0, \quad (1)$$

where $q(x, y, z)$ is the heat source that is part of the pump power, and k is the thermal conductivity of the Nd:YAG crystal. The thermal boundary conditions for equation (1) are defined by the temperature of the coolant flowing through the copper blocks between which the Nd:YAG crystal is mounted. The LASCAD program solves equation (1) numerically, to get 3D temperature profile as a result of the absorbed incident pump power. The thermal expansion in the crystal along the x, y, and z axes is also calculate according to the 3D temperature distribution. This thermal displacement profile was then used to calculate the stress induced in the crystal along the 3 axes and the equilibrium of stresses in cartesian co-ordinates as discussed in [21, 22].

This radially symmetric stress distribution with the end face of the rod having an approximately parabolic shape and the change in refractive index with temperature dn/dT, both form the thermally induced lens. In general, the various contributions to the thermal lens can be considered as closely spaced thin lenses and the total focal length of the Nd:YAG rod is given by the sum of the individual lenses. Neglecting the comparatively weak dioptric power of the stress-induced lens, the total dioptric power of the rod is given by:

$$t_{\text{thermal}} = f_{\frac{dn}{dT}} + f_{\text{endeffect}}. \quad (2)$$

The relative magnitudes of each contribution to the thermal lens is depending upon the geometry of the laser crystal and the pump characteristics.

Table 1. Physical parameters of Nd:YAG crystal [9]

Parameter	Value
Thermal conductivity (W m^{-1} K^{-1})	14
Expansion coefficient (10^{-6} K^{-1})	7.5
E-modulus (GPa)	310
Poisson's ratio	0.3
Refractive index	1.82
Thermal dispersion $\frac{dn}{dT}$ (10^{-6} K^{-1})	9.86

3. FE MODELLING CONSIDERATIONS

The FE was done for the end pumping of two Nd:YAG and YAG/Nd:YAG laser rods as sketched in Fig. 1. Figure 1a represents a homogenously doped YAG crystal with 1.1 mol % of Nd with length (L) of 14 mm and diameter of 5 mm. Figure 1b represents a composite YAG/Nd:YAG of total length of 14 mm, diameter of 5 mm and 4 mm undoped cap. The two rods are water cooled at 291 K and the two end faces are in contact with air and cooled at room temperature of 295 K.

The temperature dependence of heat conductivity was considered and accounted for and the heat transfer coefficient for air and water cooling are $h = 0.005$ and 2.0 W cm^{-2} K^{-1}, respectively. The two rods are diode pumped with a pump wavelength of 805 nm and diameter of 320 μm. The Nd:YAG physical parameters that used in the FE simulations are given in Table 1.

The fraction of pump power that converted to heat ($P_{\text{heat}} = 24.3\%$) in the laser rod is calculated according to the following formula [23]:

$$P_{\text{heat}} = \left(1 - \frac{\lambda_{\text{pump}}}{\lambda_{\text{laser}}}\right), \quad P_{\text{in}} = \left(1 - \frac{805}{1064}\right) = 24.3P_{\text{in}}, \quad (3)$$

where λ_{pump}, λ_{heat}, P_{in} are wavelength of pump light (used in the experiment), wavelength of produced laser and input pump power, respectively.

4. FE SIMULATION RESULTS

4.1. Temperature Distributions in the Nd:YAG and the Composite YAG/Nd:YAG Rods

Figure 2 illustrates FE simulations of the temperature distribution in the end pumped at 25 W of pump power (a) Nd:YAG and (b) composite YAG/Nd:YAG rods. Due to symmetry, we have presented only the upper half of each rod.

The different colors indicate different temperatures where the photons of pump powers are absorbed as shown in the color map scale. The highest value of temperature is located where the photons of pump beams enter the Nd:YAG rod (a) and after the 4 mm undoped cap of composite YAG/Nd:YAG rod (b). There is clear decrease in the temperature values in the propagation direction as the pump power absorbed. Moreover, Nd:YAG rod has a higher central temperature compared to composite laser rod at the same

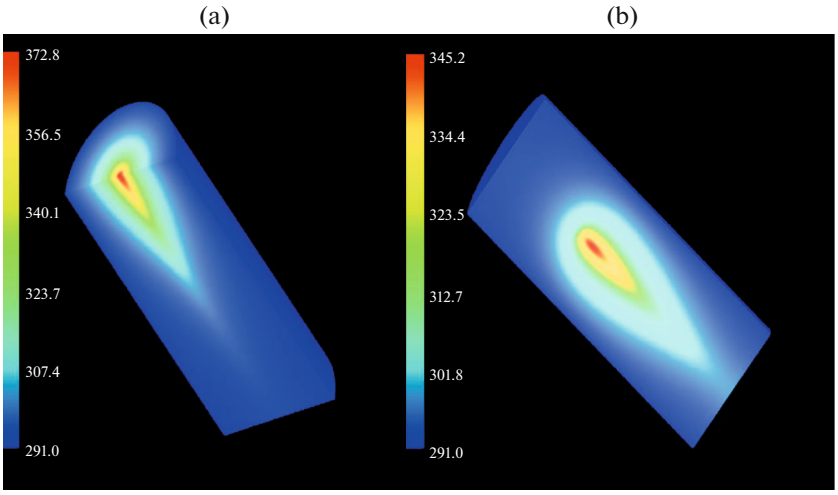

Fig. 2. Simulations of temperature distribution in for end pumped (a) Nd:YAG and (b) composite YAG/Nd/YAG rods, at 25 W of pump power.

pump power. This is because the undoped cap of the composite covering the end pump face that was in contact with air in Nd:YAG.

Figure 3 shows the semilinear dependence of the central temperature of Nd:YAG and composite YAG/Nd:YAG laser rods on pump powers. There is no remarkable change in the temperature at law powers for both rods. However, as the pump power increases, the curves tend to be slightly exponential. Further examination of the curves is not possible to maintain the rods without damaging or fracture. The slope for both curves (with linear fitting) was found to be 4.1 and 2.7 K/W for Nd:YAG and composite YAG/Nd:YAG, respectively. It is clearly seen that, the generated thermal load decreased by nearly 35% when using YAG/Nd:YAG composite laser rods due to rod conducive volume to cooling via undoped cap.

4.2. Stress Distributions in the Nd:YAG and Composite YAG/Nd:YAG Rods

The nonuniform temperature distribution has a large impact on the mechanical behavior of the material in the form of stress and strain. So, it is essential to predict the maximum incident pump powers before rupture stress occurs to the laser rod. Figure 4 shows the FE simulation results for stress intensity at 25 W of pump power (a) Nd:YAG and (b) YAG:NdYAG laser rods. The value and location of stress intensity depend on spatial distribution of temperature, material constants and the rod conductive to cooling. As can be seen in Fig. 4, that the location of maximum value of stress intensity is different for the two rods. In addition, the value of maximum stress intensity in composite YAG/Nd:YAG laser rod is slightly lower than Nd:YAG rod. We could therefore expect thermally induced crack formation to start from these positions where the stress intensity is showing to be high.

The FE calculation values of maximum stress intensity as a function of pump powers for Nd:YAG and composite YAG/Nd:YAG laser rod is presented in Fig. 5. As can be seen in Fig. 5, at low power up to 20 W the maximum value of pump intensity is nearly the same for both rods. This can be attributed to the fact that the created heat is not sufficient enough for producing long expansion of hotter central part to outer cooled parts. After approximately 20 W of pump powers, there is linear increase in the maximum stress intensity as the pump powers are raised. The maximum rupture stress value for Nd:YAG crystal is in the range 130–260 MPa [14]. Comparing the two rods at the same pump powers, the maximum stress intensity is reduced by a factor of ~30% for composite YAG/Nd:YAG laser rod. This allows power scaling while maintaining the same laser performance. The

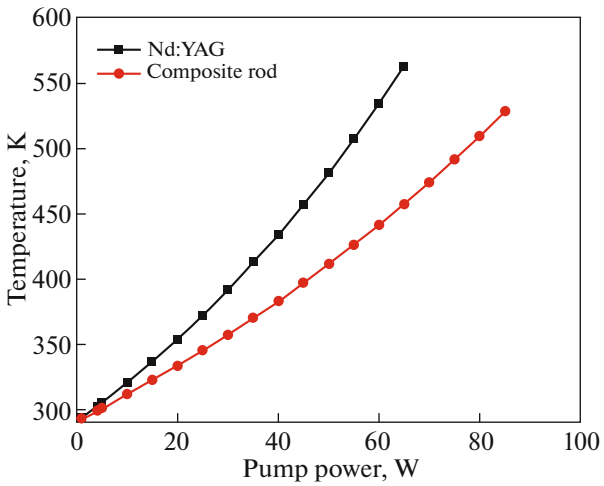

Fig. 3. Variations of the central temperature versus pump power for Nd:YAG rod and composite rod.

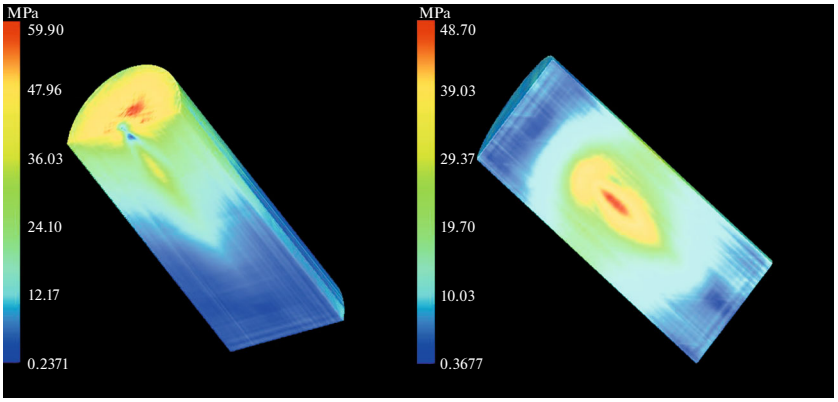

Fig. 4. Simulations of stress intensity distribution for end pumped (a) Nd:YAG and (b) composite YAG/Nd:YAG rods, at 25 W of pump power.

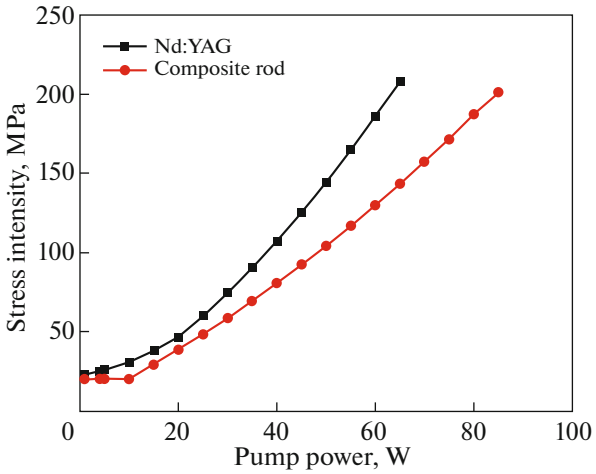

Fig. 5. Variations of the central temperature versus pump power for Nd:YAG rod and composite rod.

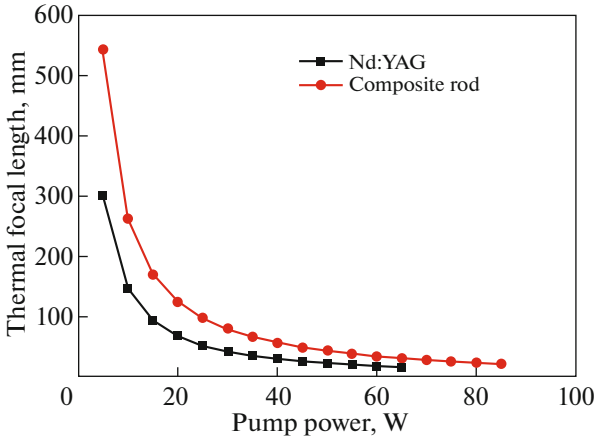

Fig. 6. The calculated thermal focal lens versus pump powers for Nd:YAG and composite YAG/Nd:YAG laser rods.

reduction in the maximum stress intensity value in using the composite YAG/Nd:YAG rather than Nd:YAG rod is due to the fact that the undoped cap has no heat generated inside it and the heat generated in the rest of the campsite rod is transferred by conduction to coolant.

4.3. Optical Path Difference and the Thermal Foal Length

The optical path difference (OPD) is given by the phase shift suffered by the propagating light through the laser rod as compared to an undisturbed medium. As presented above and due to the non-uniform temperature distribution, the OPD is a function of the transverse coordinates **x** and **y**. The calculated OPD for a beam traveling in the z-direction along the laser rod can be given by [8]:

$$\mathrm{OPD}(x,y) = \int_0^l \frac{dn}{dT} T(x,y,z)dz + (n_0 - 1)\Delta L(x,y), \quad (4)$$

the two terms in Eq. 4, where the integral are thermal dispersion and end effect, n_0 is the undisturbed refractive index of the crystal, i.e., the integrated refractive index changes along a beam path parallel to the rod axis.

In order to find the focal length of the equivalent thermal lens, the calculated $\mathrm{OPD}(x,y)$ was fitted with a parabolical $\mathrm{OPD}_{\mathrm{lens}}(r)$. The OPD of a spherical thin lens with a dioptric power D reads:

$$\mathrm{OPD}_{\mathrm{lens}}(r) = \mathrm{OPD}_0 - \frac{1}{2} r^2 D, \quad (5)$$

where r is the distance to the rod axis and OPD_0 is the optical path difference at $r = 0$.

The calculations of thermal focal length of thermally induced lens in the Nd:YAG and composite

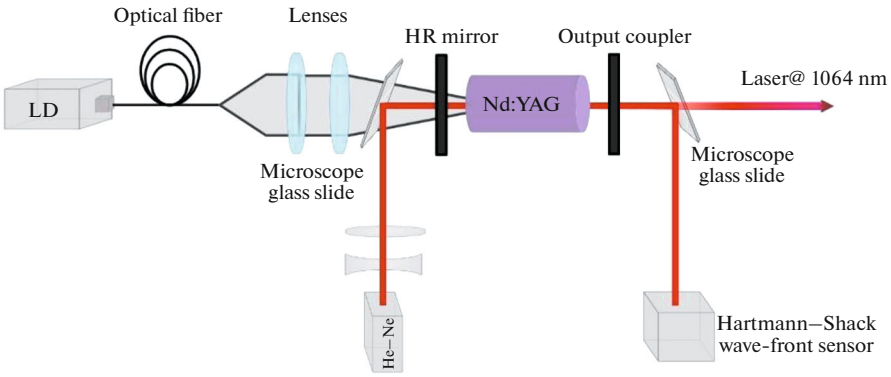

Fig. 7. Experimental setup.

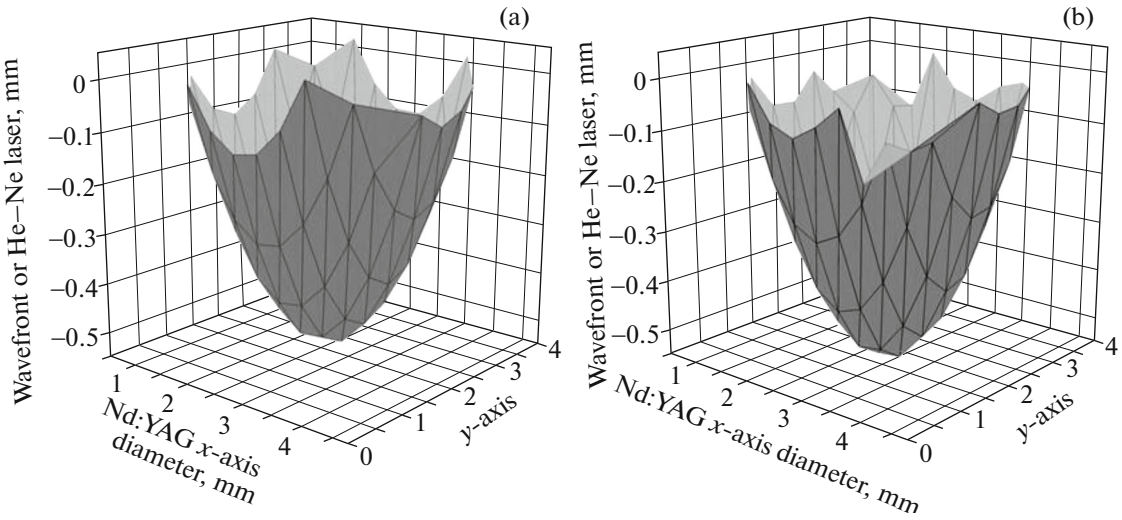

Fig. 8. Wavefront measured with Hartmann–Shack sensor for Ne–Ne laser beam passing pumped (a) Nd:YAG and (b) composite YAG/Nd:YAG rods pumped at 20 W.

YAG/Nd:YAG laser rods are presented in Fig. 6. The calculated values in Fig. 6 showed that higher pump powers lead to stronger thermal lens of shorter focal length for both rods. At low level of pump powers of 1–30 W, the Nd:YAG rod suffers from stronger thermal lens than composite YAG/Nd:YAG laser rod. This mainly due to neglecting the contribution of end effect in the composite YAG/Nd:YAG laser rod through the undoped cap.

5. EXPERIMENTAL

The experimental setup for producing laser and wavefront measurement aberration for thermally induced lens is shown in Fig. 7. The light from the laser diode operating at 805 nm is coupled into a large core optical fiber of a fiber core diameter of 400 μm and numerical aperture of 0.22. A set of focusing lenses were used to configure a nearly circular beam spot of size ~320 μm on the laser rod. The laser rod (Crytur no. P3363 [24]), barrel surface fine ground end faces polished flat $<\lambda/10$, parallel each other <10 arcsec, perpendicular to the rod axis <5 arcmin, surface S/D 10/5 both sides coated with AR for 1064 nm and HT for 808 nm and then is wrapped with an indium foil and mounted in a copper holder. The mounted laser rod is cooled by water at a 295 K. The input pump beam was focused at ~0.5 mm of the free end of Nd:YAG laser rod and at ~4 mm for composite YAG/Nd:YAG laser rod. Two parallel mirrors were used during the experiment with input coupling mirror having high transmittance (HT > 99%) for the pump wavelength at 805 nm and a high reflectivity (HR > 99.5%) at laser wavelength at 1064 nm. The laser output coupling mirror has ~5% transmittance at 1064 nm.

For the measurements of the focal length of thermally induced lens, a He–Ne laser beam is magnified to cover a ~4 mm of rod diameter and reflected to the laser by a microscope glass slide. After the He–Ne laser beam has passed the laser rod, it is reflected back

Table 2. Comparison between FE simulation results for thermal focal length of thermally induced lens in the Nd:YAG and composite YAG/Nd:YAG laser rods

Pump power, W	FE-simulation f, mm		Hartmann–Shack				$\pm\delta f$	
	Nd:YAG	YAG/Nd:YAG	Nd:YAG		composite YAG/Nd:YAG		Nd:YAG	YAG/Nd:YAG
			f_x, mm	f_y, mm	f_x, mm	f_y, mm		
5	300	542	290	275	500	475	0.06	0.10
10	145	263	135	128	250	240	0.09	0.07
15	93	170	83	75	155	148	0.15	0.11
20	68	124	60	55	115	110	0.15	0.09
25	52	97	45	42	88	82	0.16	0.12
30	42	79	38	34	68	64	0.14	0.16
40	30	56	26	23	51	47	0.18	0.13
50	22.6	42.9	19	17	38	34	0.20	0.16

by a microscope glass slide to the Hartmann–Shack senor (WFS1505C-Thorlabs) for measuring wavefront aberrations occurred due to the presence of thermal lens.

The Hartmann–Shack wavefront sensor was calibrated by a spherical converging lens of 50 mm focal length on a translation stage at different positions. The error in measurements was in the range of ~10%. After calibration, we have measured the wavefront of He–Ne laser beam after passing the unpumped Nd:YAG laser rod and recorded as a flat reference shape of wavefront.

Figure 8 shows the deformation that happened in the wavefront of He–Ne laser beam after passing the pumped (a) Nd:YAG and (b) composite YAG:NdYAG laser rods. The deformation is high at the center of the rods and decreased gradually to the circumference of the rods. The measurements cover only the area that covered by He–Ne laser from the whole laser rods. This deformation represents the OPD. The parabolic shape OPD in Fig. 8, is fitted to a second order polynomial as presented in [25, 26].

Depending on the shape of pump light and its distribution in the laser rod, the thermal lens may not be radially symmetric. This produces an astigmatic thermal lens with two focal lengths f_x and f_y.

The comparison between the FE numerical calculations for focal lens of thermally induced lens and the experimental validation for Nd:YAG and composite YAG/Nd:YAG laser rods are presented in Table 2. The uncertainty of the present finding listed in columns 8 and 9 in Table 2, they are assisted using the formula of:

$$\delta f = \frac{|f_{FE} - f_{exp}|}{\max(f_{FE}, f_{exp})}, \quad (6)$$

where, f_{FE} is the calculations for focal lens of thermally induced lens and f_{exp} is the experimental results by using Hartmann–Shack sensor for Nd:YAG and composite YAG/Nd:YAG laser rods.

The variation between measurements and calculations can be refer to the accuracy of the FE analysis which is given by two points and the numerical resolution of the algorithm that affected by the values of the input parameters. Moreover, the adjustment of focal point of pump light can be misplaced during replacement of the Nd:YAG and composite YAG/Nd:YAG laser rods.

6. CONCLUSIONS

We have numerically investigated the thermal effects in end-pumped solid-state Nd:YAG cylindrical laser rods. We have analyzed the temperature distributions and stress distribution based on FE numerical modelling simulation program for Nd:YAG and composite YAG/Nd:YAG laser rods. We have also presented the calculated data of focal length of created thermally induced lens for both rods at different pump powers. The FE simulations showed that the stress intensity and thermal focal length are mitigated by using composite laser rod by nearly about ~35% and ~50%, respectively. In addition, we can determine the location of maximum stress intensity that can lead to laser rod fracture.

Using composite laser rod of undoped section with neodymium (Nd) is capable for mitigating the focal length of thermally induced lens and stress intensity by a 1/3 and a 1/5, respectively. We have validated the FE simulations calculation by direct measurements of focal length of thermally induced lens. The experimental measurements by using Hartmann–Shack wavefront sensor were agreed well with the FE calculations.

FUNDING

This work was done with the support of Taif University Researchers Supporting Project TURSP-2020/25, Taif University, Taif, Saudi Arabia.

REFERENCES

1. L. A. Ngiejunbwena et al., Opt. Laser Technol. **133**, 106528 (2021).
2. N. A. Vainos et al., Nanomaterials **11**, 35 (2021).
3. A. A. Menazeaa and A. M. Abdelghanya, Radiat. Phys. Chem. **174**, 108958 (2020).
4. D. A. O. Modena et al., Lasers Med. Sci. **35**, 797 (2020).
5. D.-L. Kima et al., Optik **181**, 1085 (2019).
6. Ch. Song et al., Opt. Commun. **478**, 126378 (2021).
7. S. Chenet et al., Prog. Quantum Electron. **30**, 89 (2006).
8. A. K. Cousins, IEEE J. Quantum Electron. **28**, 1057 (1992).
9. W. Koechner, *Solid-State Laser Engineering* (Springer, New York, 2006).
10. V. A. Desyatskov, L. V. Desyatskova, and A. V. Stepanov, Herald Bauman Moscow State Tech. Univ., Ser. Instrum. Eng., No. 4, 12 (2009).
11. A. N. Zakharova, P. A. Loiko, A. M. Malyarevich, and K. V. Yumashev, Devices Methods Meas. **6** (2), 127 (2015).
12. A. V. Morozov and I. I. Pakhomov, Herald Bauman Moscow State Tech. Univ., Ser. Instrum. Eng., No. 2, 3 (2004).
13. G. V. Kuptsov, A. V. Laptev, V. A. Petrov, V. V. Petrov, and E. V. Pestryakov, Bull. Sib. State Univ. Geosyst. Technol. **24** (2), 220 (2019).
14. R. Bhushan et al., Jpn. J. Appl. Phys. **46**, 1051 (2007).
15. X. Yu et al., Opt. Lett. **42**, 2730 (2017).
16. I. Snetkov and O. Palashov, Opt. Mater. **42**, 293 (2015).
17. D. Asoubar and F. Wyrowski, Opt. Express **23**, 18802 (2015).
18. LASCAD Gmbh, https://www.las-cad.com/index.php.
19. J. M. Eggleston, T. J. Kane, K. Kuhn, J. Unternahrer, and R. L. Byer, IEEE J. Quantum Elecron. **20**, 289 (1984).
20. H. S. Carlslaw and J. C. Jaeger, *Conduction of Heat in Solids* (Clarendon, Oxford, 1989).
21. X. Peng et al., Appl. Opt. **40**, 1396 (2001).
22. LASCAD GmbH. LASCAD 3.6 Manual (January 2014). https://www.las-cad.com/lascad_documentation.php.
23. J. Yang and J. Liu, Optik **115**, 538 (2004).
24. Crytur, Integrated crystal based solutions. https://www.crytur.cz
25. R. M. El-Agmy and N. Al-Hosiny, Photonic Sens. **7**, 329 (2017).
26. R. M. El-Agmy and N. Al-Hosiny, Optik **140**, 584 (2017).